Journal of The Electrochemical Society, **150** (1) B16-B25 (2003)
0013-4651/2002/150(1)/B16/10/$7.00 © The Electrochemical Society, Inc.

Chromate Conversion Coatings Formation on Zinc Studied by Electrochemical and Electrohydrodynamical Impedances

A. A. O. Magalhães,[a,b] B. Tribollet,[b,*] O. R. Mattos,[a,*,z] I. C. P. Margarit,[a,c] and O. E. Barcia[d]

[a]*Programa de Engenharia Metalurgica e de Materials/Dipartamento de Engenharia Metalúrgica e de Materials/Instituto Alberto Luiz Coimbra de Pòs Graduação e Pequìsa de Engenharia, Escola de Engenharia Universidade Federal do Rio de Janeiro, Rio de Janeiro, Brazil*
[b]*Unité Propre de Recherche 15 du Centre National de la Recherche Scientifique/Physique des Liquides et Electrochimie, Université Paris VI, Paris, France*
[c]*Escola de Química Departamento de Processos Inorgânicos,* [d]*Instituto de Química, Departamento de Fisíco-Química, Universidade Federal do Rio de Janeiro, Rio de Janeiro, Brazil*

The formation of chromate conversion coatings on zinc was studied by chronopotentiometric, electrochemical, and electrohydrodynamic impedances, and interfacial pH measurements. The electrochemical experiments were performed with a rotating disk electrode of pure zinc, and the pH measurements were obtained with a zinc deposit on a gold grid electrode in a submerged impinging jet cell. The electrolyte was an industrial chromate bath. The experimental results were achieved for different immersion times, temperatures, and rotation speeds. Kinetic reactions and physical model for the chromate layer formation on zinc were proposed, and the electrochemical and electrohydrodynamic impedances were well simulated.
 [DOI: 10.1149/1.1528196]

Manuscript submitted January 18, 2002; revised manuscript received July 22, 2002. Available electronically December 13, 2002.

Several sectors of automobile, aerospace, and electrical appliances industries improve the anticorrosive properties of their galvanized products by application of chromate conversion coatings on zinc deposits. The objective is to decrease the formation of corrosion products, and, thereby, to avoid modification of their properties during transportation and storage. The conversion treatments can also act as a support for the application of painting if direct adherence of the organic coatings on the substrate is not satisfactory. The principle of a conversion treatment consists basically in transforming the surface of the metallic substrate from the active state to the passive state. The formed layer is composed of a combination of reduced species products from ions present in the conversion bath and, in smaller quantities, corrosion products from the substrate.

The chromate coating is usually applied on galvanized steels through simple immersion in an acidic solution that contains chromium hexavalent species. The quality and the efficiency of these layers are strongly dependent on the bath composition, the surface of substrate, and the parameters of the process. Many studies in the literature concern the mechanisms of deterioration and the development of control and assessment methods for the quality of these conversion layers.[1-8] Even though chromatation is used in industry its deposition mechanism is not yet completely understood.

The chemical composition of these layers is not yet well defined; the difficulties of a composition survey of this type are due mainly to the thinness of the layers. The main parameters that control the composition of the chromatation layers on zinc are the quality of the zinc surface, the composition of the bath, the pH of the solution, the immersion time in the bath, the bath temperature, and the thickness of the layer. According to the majority of works, the main constituent of the formed layer is trivalent chromium in the form of oxides,[9-12] hydroxides,[4,7,13] and complex.[3,14,15] The hexavalent chromium species is found in least quantity in the form of complex compounds with trivalent chromium or simply absorbed in the layer. Only trace amounts of zinc and such activator anions as phosphates, nitrates, sulfates, chlorides, and fluorides are present.

Although there are a great variety and complexity of reactions proposed for the zinc/chromate solution interface,[16] this formation obeys a zero net current as a result of the compensation of a reduction component from the electrolyte and an oxidization component of the metal. A consensus exists in the literature that maintains that the two main stages for the formation of a layers of chromatation are the dissolution of zinc in an acidic electrolyte and the formation of a precipitate of trivalent chromium.

Trivalent chromium can form different types of oxides and/or hydroxide compounds. During reduction of hexavalent chromium there is a consumption of H^+, which increases the local pH and allows precipitation of a gel-like film.

The aim of this work is to employ infrequently used modern electrochemical techniques in the chromatation process studies. We hope that this approach can be useful for further research concerning nontoxic alternatives for conversion baths.

Experimental

All the electrochemical measurements were performed with a three-electrode cell. The working electrode was manufactured from pure zinc (99.9%) rod. This electrode was covered by a cataphoretic paint and coated with a resin epoxy to expose a 0.27 cm^2 cross-sectional area to the electrolyte. The electrode surface treatment protocol consisted of polishing with emery paper 600 and 1200, rinsing with double-distilled water, rinsing with ethanol, and finally drying with air. The reference electrode was a saturated calomel electrode (SCE) and the counter electrode was a large platinum grid.

The electrolytic solution was a 5% v/v solution of a concentrated commercial product, which consisted primarily of sodium chromate and sulfuric acid. This solution is used in the chromatation step of an electrogalvanized steel industrial process in a Brazilian metallurgy society. The chromate conversion coatings formed by this solution with temperature between 47 and 48°C and pH between 2.96 and 3.00, showed good corrosion resistance as presented previously.[1]

The electrochemical tests were conducted at pH 3.0, at temperatures of 25 and 47°C, controlled by a thermostatic bath.

The zinc rotating disk electrode (RDE) open-circuit potential (OCP) evolution in the chromate solution was achieved using a potentiostat Ominimetra model PG-19 for 30 min of immersion for four different rotation speeds (0, 250, 500, and 1000 rpm). A dc motor with a servo system controlled the RDE and the rotation rate was measured with a tachometer made by Asservissement Eletronique under a CNRS/France license. The ac impedance measurements were conducted at the OCP of the system under potentiostatic regulation at three different immersion times: 2, 15, and 30 min, and three rotation speeds: 250, 500, and 1000 rpm. The electrohydrodynamic impedance spectroscopy (EHD) measurements were conducted under potentiostatic regulation. The rotation rate was initially fixed at 1000 rpm, and after 15 and 30 min of immersion, the OCP

* Electrochemical Society Active Member.
z E-mail: Omattos@metalmat.ufrj.br

corresponding to this rotation was applied and the measures were done reducing the rotation rates. The rotation rates measured were 240, 480, and 720 rpm. The ac impedance measurements were obtained for frequencies varying from 65 kHz to 100 mHz using a sinusoidal amplitude of 10 mV applied by the generator of a frequency-response analyzer (FRA, Solartron 1250) controlled with an IBM PC using software developed in the UFRJ Corrosion Laboratory in Brazil. For EHD measurements, a sinusoidal speed modulation of 10% around a mean value was applied by the system described above.

The interfacial pH measurements were obtained using a working electrode with an 82 mesh gold grid (Goldfellow, wire diam: 0.06 mm, open area 64%). A 0.5 mm diam gold wire was welded onto the periphery of the gold grid to provide an electrical connection. A zinc deposit was formed on the gold grid using a solution of 350 g/L of $ZnSO_4 \cdot 7H_2O$ and 30 g/L $(NH_4)_2SO_4$ pH 4.0 at 25°C and a current density of 180 mA/cm^2 for 7 min. After deposition, the grid was dried with an argon jet and contacted with the flat end of a combined pH electrode and fixed to the lateral wall of the pH electrode with Teflon tape. The pH electrode/zinc deposit grid electrode assembly was fixed in a submerged impinging jet cell. The jet cell and all the pH setup are the same as used by Deslouis *et al.*[17] The OCP of the grid electrode in the chromate solution was monitored against a saturated sulfate electrode (SSE) with an electronic potentiostat (Sotelem) and the pH was measured simultaneously with a pH meter (LPH 230T Radiometer).

Results and Discussion

OCP.—Figure 1 presents the evolution of the OCP as a function of immersion time in the chromate solution for the stationary electrode (0 rpm) and with rotation speeds of 250, 500, and 1000 rpm at 25 (Fig. 1a) and 47°C (Fig. 1b). During the first seconds of immersion at 47°C, the potential decreased toward more cathodic values. After this reduction, the potential stabilized for all rotation speeds to values close to −1.32 mV, and the potential remained steady during the entire immersion time. It is supposed then that the film covers the substrate surface completely, and the dissolution of zinc continues to take place through the formed layer. The potential stabilization speed is greater for the smallest rotation speeds. The potential of a stationary electrode stabilizes more quickly than the potential of an electrode rotating at a speed of 1000 rpm. This behavior is more evident when the temperature of the solution is reduced. The potential curves at 25°C are presented for the same rotation speeds as shown for 47°C. The influence of the speed variation of the electrode in the process appears more clearly, it changes not only the time of stabilization, but also the values of the potential. With these results it is possible to identify some effects of temperature and mass transport in the process. First, the rotation speed influences film formation, maybe acting on zinc dissolution rate at the interface. Second, the temperature, when it increases from 25 to 47°C, provides an increase of the zinc dissolution velocity, which is almost the same for all rotations tested.

AC and EHD impedance measurements.—The electrical impedence spectroscopy (EIS) diagrams obtained during the chromatation process are presented in Fig. 2. The diagrams present a relatively complex shape that suggest the presence of two capacitive loops at high frequencies (HF) followed by an inductive loop at low frequencies (LF). The first capacitive loop at higher frequencies is assigned to the charge-transfer resistance of the electrochemical reactions in parallel with the double layer (dl) capacitance. The second capacitive loop at intermediate frequencies presents a slight inclination that could correspond to a diffusion phenomena. This diffusion could take place in the electrolyte and/or in the chromate film.

The increase of the size of the diffusive loop with immersion time of the electrode in the solution (see Fig. 2a and b) can be explained by diffusion in a layer of increasing thickness, by diffusion in a porous film in which the pores contract or by diffusion in a gel-like film that becomes increasingly cross-linked. The low frequency limit of the impedance associated to diffusion is directly proportional to the thickness of the layer. The reduction of the size of the capacitive diffusive loop when the rotation speed of the electrode increases (see Fig. 2c and d) can be assigned to diffusion within the solution and/or to diffusion through a film whose thickness decreases with the rotation speed. This last hypothesis probably can occur if the layer is a gel-like film.

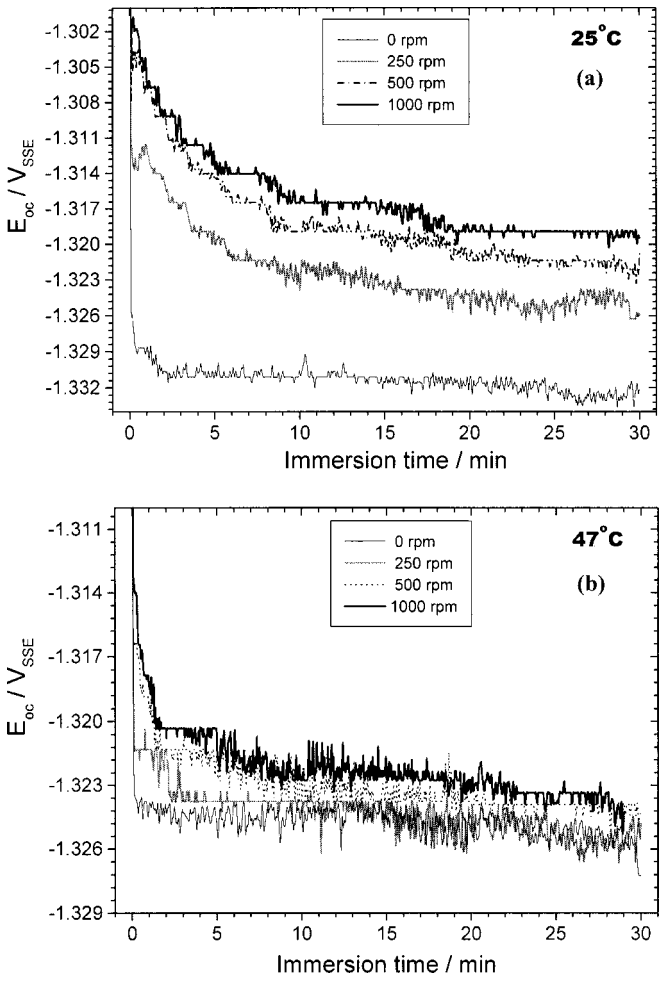

Figure 1. OCP of zinc RDE in function of immersion time in the chromate solution at (a) 25 and (b) 47°C.

Due to the mixed potential of the electrode, the inductive loop can be explained by either considering the anodic component separately from the cathodic (adsorption of an activating species or desorption of a blocking species with increasing overpotential of each component) or considering the adsorption of only one and same species interacting with the two components. Two cases can be considered: (*i*) the anodic adsorption (therefore cathodic desorption) of a blocking species for the two reactions (passive layer). The inductive loop appears then if the dominant effect is in the cathodic component or (*ii*) or the anodic desorption (therefore cathodic adsorption) of a blocking species for the reactions (chromate layer). The inductive loop appears then if the dominant effect is in the anodic component.

Only a weak effect of temperature is seen in these impedance diagrams by comparing the diagrams obtained at 25 (Fig. 2b and d) and 47°C (Fig. 2a and c). Therefore, it can be considered that the effect of the mass transport in this system has a higher influence than the temperature effect in the kinetics of chromate film formation. Thus, the EHD technique seems well adapted to this problem.

Figure 3 presents the EHD of zinc RDE immersed in the chromate solution at 25 and 47°C. The shape of the experimental dia-

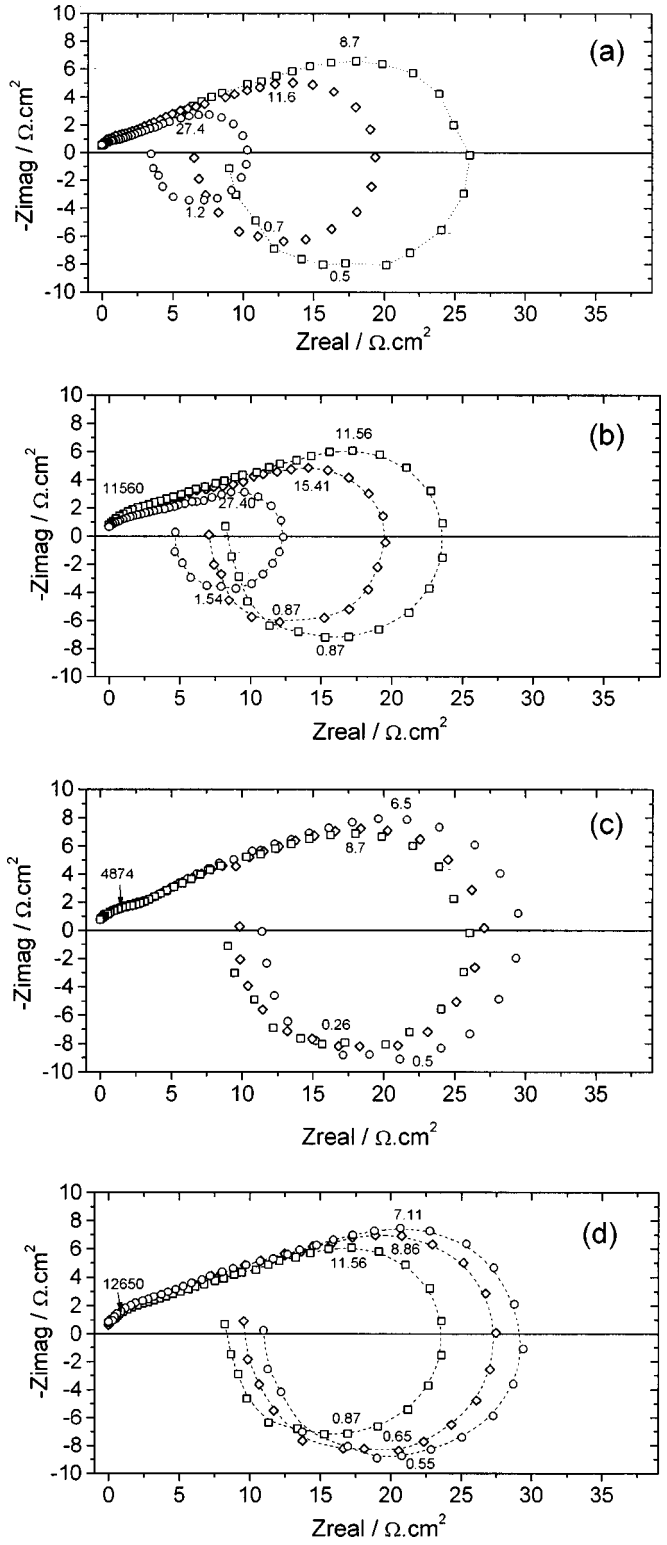

Figure 2. Experimental electrochemical impedances diagrams at 1000 rpm after (-○-) 2, (-◇-) 15, and (-□-) 30 min of immersion in the solution at (a) 47°C (a) and (b) 25°C and diagrams after 30 min at (-○-) 250, (-◇-) 500, and (-□-) 1000 rpm in the solution at at 47°C (c) and (d) 25°C (frequencies in hertz).

gram at 25°C (Fig. 3a) shows two time constants, one at low frequencies and another at high frequencies, that do not vary with the increase of the immersion time. In a preliminary analysis, such observations indicate that the chromate layer is partially blocking. The

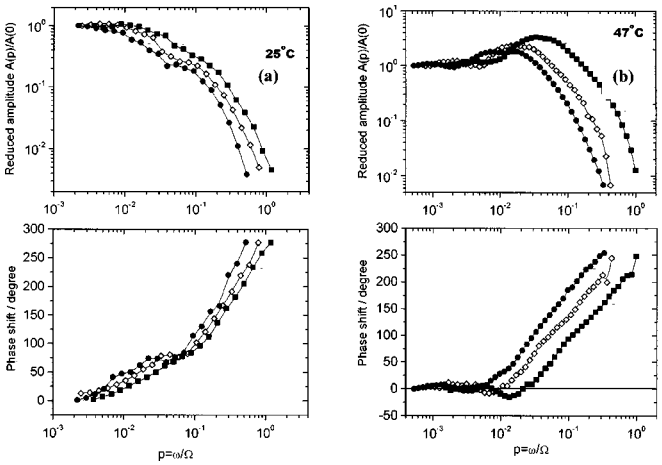

Figure 3. Experimental EHD diagrams after 15 min immersion in the solution at (a) 25 and (b) 47°C. (-●-) 240, (-◇-) 480, and (-■-) 720 rpm.

shift of characteristic frequencies toward lower values as rotation speed increased is qualitatively consistent with diffusion through a porous layer.[18] In conclusion, this qualitative analysis in the shape of the EHD seems to show that the layer of chromatation possesses a mixed behavior in relation to diffusion. The diffusion is affected by both a partially blocked electrode and a porous layer. However, at 47°C (Fig. 3b), the behavior is quite different from that seen at 25°C; an increase of the impedance modulus at intermediate frequencies is observed. Such behavior was never modeled for any system. We proposed a model that takes into account the oxidization of zinc and the reduction of Cr^{6+} simultaneously, where the process of film formation occurs at the OCP in the electrode interface.

Local pH measurements.—Figure 4 shows the behavior of the pH interfacial and the rest potential of the gold grid with zinc deposited in the chromate solution. At immersion of the electrode in the solution, a reduction of pH occurs, and, after some seconds, a plateau is seen around pH 4.0. At the same time, there is a reduction of the potential followed by a plateau around $-1.32\ V_{sse}$.

The pH of the bulk solution is 3.0, so the elevated pH plateau shows that there is consumption of H^+ at the zinc/electrolyte interface. Such behavior is in agreement with the literature, which shows consumption of H^+ at the interface providing the precipitation of trivalent chrome products on the zinc surface.[4,6,19] The potential plateau is the same as obtained for the pure zinc electrode (Fig. 1) and corresponds to the formation of chromate film on a zinc surface that dissolves at the same time. After the first pH plateau there is an abrupt reduction for values around pH 3.2 that corresponds to direct contact of the solution with the gold substrate. This is due to the dissolution of the zinc in the electrode, masking the value of actual pH on the surface of the remaining zinc. After 15 min of immersion, the potential begins to increase indicating, at the end of the test, that the zinc is totally dissolved from the surface electrode. The pH stays at the value of bulk solution.

Kinetic and Physical model

The chemistry of chromate baths is complex and involves many equilibrium reactions.[20] However, the chromatation itself occurs as a heterogeneous process at the metal/solution interface. In this case, anodic reactions play an important role. Due to the complexity of the process, it is difficult to generalize results obtained with aluminum[21] or others metals to this study concerning zinc. Actually, the interfacial pH of electrochemical processes depends significantly on the metal and/or bath.[22]

The model proposed below is very simple and did not take into account the complexity of the chromatation process. Moreover, a kinetic model is never unique and the main purpose of this model is

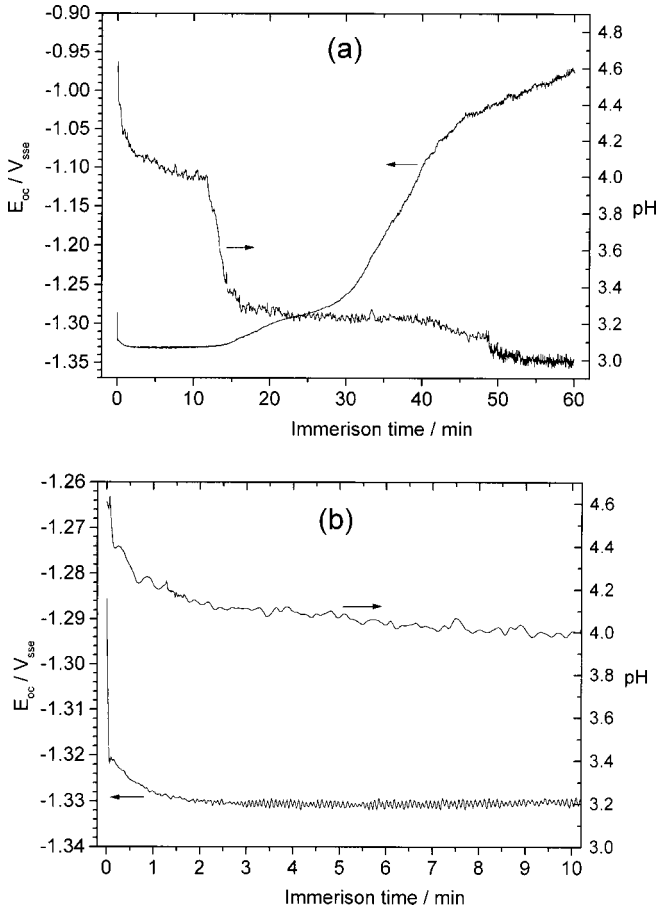

Figure 4. OCP and pH evolution of a zinc electrodeposited grid in the chromate solution during (a) entire time of measurements and (b) the first 10 min.

to verify whether the qualitative ideas presented during the analysis of the new results obtained by ac and EHD can be supported by an electrochemical model.

The proposed kinetic reaction model considers the following reactions

$$\mathrm{Zn} \xrightarrow{k_1} \mathrm{Zn^{2+}} + 2\mathrm{e^-} \quad [1]$$

$$\mathrm{Zn} + \mathrm{H_2O} \underset{k_{22}}{\overset{k_2}{\rightleftarrows}} \mathrm{ZnO_{(\theta)}} + 2\mathrm{H^+} + 2\mathrm{e^-} \quad [2]$$

$$\mathrm{CrO_4^{2-}} + 5\mathrm{H^+} + 3\mathrm{e^-} \xrightarrow{k_3} \mathrm{Cr(OH)_3} + \mathrm{H_2O} \quad [3]$$

$$\mathrm{Zn} + \mathrm{ZnO_{(\theta)}} \xrightarrow{k_4} \mathrm{Zn^{2+}} + \mathrm{ZnO_{(\theta)}} + 2\mathrm{e^-} \quad [4]$$

The first reaction corresponds to zinc dissolution. The second reversible reaction corresponds to zinc oxide formation[4,14] as an insoluble adsorbed species whose surface coverage is θ. The third reaction corresponds to a formation of a precipitated trivalent chromium [assumably $Cr(OH)_3$] product from the reduction of hexavalent chromium species and consumption of H^+. This reaction can be replaced by any other source of Cr(VI), for example $Cr_2O_7^{2-}$. For the present purpose we need only a Cr(VI) source and, as we are working with Na_2CrO_4, Reaction 3 was taken. The last reaction is an autocatalytic reaction of zinc dissolution. A reaction as $Cr(VI)^{x-} + 4H^+ + 3e \rightarrow Cr(OH)_3 + yH_2O$ could well be used replacing Reaction 3.

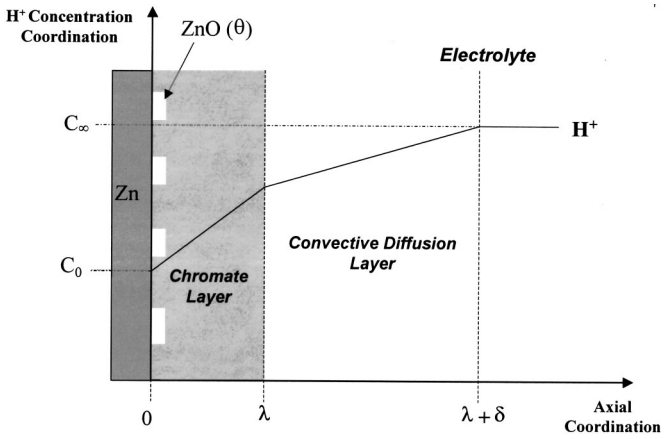

Figure 5. Physical model scheme for the formation of chromate conversion layer on Zn in an acid chromate solution.

The H^+ concentration gradient (Fig. 5) is distributed between the chromate layer, where mass transport is controlled by molecular diffusion, and the electrolyte diffusion layer, where mass transport is controlled by convective diffusion. For this model, the transport becomes one-dimensional (1-D, along the axial coordinate of RDE) where λ is the chromate layer thickness, δ is the diffusion layer thickness, C_∞ is the concentration of the H^+ in the bulk solution, and C_0 the concentration of H^+ at the zinc/chromate layer interface.

Steady-state equations.—From the model of four kinetic reactions proposed above the steady-state faradaic current may be obtained

$$\frac{i}{F} = 2k_1(1-\theta) + 2k_2(1-\theta) - 2k_{22}\beta\theta C_0^2 - 3k_3(1-\theta) \times [\mathrm{CrO_4^{2-}}]C_0^5 + 2k_4\beta\theta \quad [5]$$

where ZnO is an insoluble adsorbed species whose surface coverage is θ, β being the total number of sites available for adsorption. F is the Faraday number, and the rate constants k_i obey the Tafel law, which are written in the standard way: $k_i = k_{i0}\exp(b_iE)$, with $b_i = nF/RT$. The mass balance for the ZnO species is

$$\beta\frac{d\theta}{dt} = k_2(1-\theta) - k_{22}\beta\theta C_0^2 \quad [6]$$

Under the assumption of a steady state ($d\theta/dt = 0$) and that Reaction 2 is at equilibrium

$$\theta = \frac{k_2}{k_2 + k_{22}\beta C_0^2} \quad [7]$$

The overall steady-state current is equal to zero ($i = 0$). k_{30} can be derived from Eq. 5 as

$$k_{30} = \left(\frac{2k_1k_{22}C_0^2 + 2k_4k_2}{3k_{22}[\mathrm{CrO_4^{2-}}]C_0^7}\right)\exp(b_3E) \quad [8]$$

Under these conditions, the H^+ consumption is due only to Reaction 3. By taking into account Eq. 7, the H^+ flux is given by

$$D_f\left.\frac{d\overline{C}_{H^+}}{dy}\right|_0 = \frac{5k_3k_{22}\beta[\mathrm{CrO_4^{2-}}]C_0^7}{k_2 + k_{22}\beta C_0^2} \quad [9]$$

where D_f is the diffusion coefficient relative to the chromate film. The H^+ flux at the surface can be expressed as

$$D_f \frac{d\overline{C}_{H^+}}{dy}\bigg|_0 = D_f \frac{C_\lambda - C_0}{\lambda} = D_s \frac{C_\infty - C_\lambda}{\delta} \quad [10]$$

where D_s is the diffusion coefficient relative to the electrolyte diffusion layer, and C_λ is the H^+ concentration at the interface chromate layer/electrolyte. Thus

$$D_f \frac{d\overline{C}_{H^+}}{dy}\bigg|_0 = \frac{\frac{D_f}{\lambda}}{\frac{D_f}{\lambda} + \frac{D_s}{\delta}}\left(D_s \frac{C_\infty - C_0}{\delta}\right) = \frac{5k_3k_{22}\beta[CrO_4^{2-}]C_0^7}{k_2 + k_{22}\beta C_0^2} \quad [11]$$

Under assumptions that $C_\infty \gg C_0$ and $\theta \ll 1$ ($k_2 \ll k_{22}\beta C_0^2$)

$$\frac{\frac{D_f}{\lambda}}{\frac{D_f}{\lambda} + \frac{D_s}{\delta}}\left(D_s \frac{C_\infty}{\delta}\right) = 5k_3[CrO_4^{2-}]C_0^5 \quad [12]$$

and an expression can be obtained for C_0 that is a function of rotation speed and potential of the electrode [$C_0 = f(\Omega,E)$]

$$C_0 = \left[\frac{\frac{D_f}{\lambda}}{\frac{D_f}{\lambda} + \frac{D_s}{\delta}}\left(D_s \frac{C_\infty}{\delta}\right)\frac{1}{5k_3[CrO_4^{2-}]}\right]^{1/5} \quad [13]$$

where

$$\delta = \left(\frac{3D_s}{0.51023v}\right)^{1/3}\sqrt{\frac{v}{\Omega}} \quad [14]$$

Nonsteady-state equations.—The concentration distribution in the diffusion layer is governed by the 1-D nonsteady equation of convective diffusion, such that the usual mass-balance equation can be integrated in the electrolyte on a normal distance to the chromate layer

$$\frac{\partial C_{H^+}}{\partial t} + V_y \frac{\partial C_{H^+}}{\partial y} = D_s \frac{\partial^2 C_{H^+}}{\partial y^2} \quad [15]$$

The development of V_y is provided in Ref. 23, 24. Upon introducing $C_{H^+} = \overline{C}_{H^+} + Re\{\tilde{c}\exp j\omega t\}$ and in terms of the dimensionless variables and parameters: (*i*) $a = 0.51023$, (*ii*) $\eta = y/\delta$, (*iii*), and (*iv*) $\xi = \omega\delta^2/D = 3.258\, pSc^{1/3}$. Where $Sc = \upsilon/D_s$ is the Schmidt number, and the equivalent Nernst diffusion layer thickness is $\Gamma(4/3)$ times δ, Eq. 15 becomes

$$\frac{d^2\tilde{C}_{H^+}}{d\eta^2} + 3\eta^2\frac{d\tilde{C}_{H^+}}{d\eta} - j\xi\tilde{C}_{H^+} = -\frac{\Delta\Omega}{\overline{\Omega}}\frac{3\tilde{f}'(p)}{a}\eta^2 D_s\frac{d\tilde{C}_{H^+}}{d\eta}$$

where

$$\frac{d\overline{C}_{H^+}}{d\eta} = \frac{C_\infty - C_\lambda}{\Gamma(4/3)}\exp - \eta^3 \quad [16]$$

By using the same procedure as described in Ref. 23, 24, the convective diffusion equation for H^+ is obtained as

$$\frac{d\tilde{C}_{H^+}}{dy}\bigg|_{\lambda^+} = \frac{\tilde{C}_\lambda\theta'(0)}{\delta} + \frac{\Delta\Omega}{\overline{\Omega}}\frac{d\overline{C}_{H^+}}{dy}\bigg|_{\lambda^+} W_H \quad [17]$$

where the function W_H corresponds to the EHD given in Ref. 23, 24 as $W_0(\xi)$ and $-1/\theta'(0)$ is the usual dimensionless convective diffusion impedance which is a function of the dimensionless frequency p (ω/Ω) and the Schmidt number of the diffusing species.[23,24] Position λ^+ indicates the concentration gradient in the electrolyte.

Chromate layer/electrolyte interface.—At the chromate layer/electrolyte interface, the balance of the flux of H^+ is given by

$$D_s \frac{d\tilde{C}_{H^+}}{dy}\bigg|_{\lambda^+} = D_f \frac{d\tilde{C}_{H^+}}{dy}\bigg|_{\lambda^-} \quad [18]$$

where λ^- indicates the concentration gradient in the chromate layer.

Diffusion in the chromate layer.—In the chromate layer, the diffusion of H^+ ion is given by

$$\frac{\partial C_{H^+}}{\partial t} = D_f \frac{\partial^2 C_{H^+}}{\partial t^2} \quad [19]$$

By using an axial dimensionless distance defined by

$$\chi = \frac{y}{\lambda}$$

$$\left(\frac{\partial C_{H^+}}{\partial t}\right)_y = \left(\frac{\partial C_{H^+}}{\partial t}\right)_\chi \quad [20]$$

The diffusion equation becomes

$$\frac{\partial^2\tilde{C}_{H^+}}{\partial\chi^2} = j\mu\tilde{C}_{H^+}$$

where

$$\mu = \frac{\omega\lambda^2}{D_f} \quad [21]$$

The general solution is

$$\tilde{C}_{H^+} = G\exp\sqrt{j\mu}\chi + H\exp - \sqrt{j\mu}\chi \quad [22]$$

where G and H may be obtained by considering the boundary conditions.

At the zinc interface ($\chi = 0$)

$$\tilde{C}_0 = G + H$$

and

$$\frac{\partial\tilde{C}_{H^+}}{\partial\chi}\bigg|_0 = \sqrt{j\mu}(G - H) \quad [23]$$

Thus

$$\frac{\partial\tilde{C}_{H^+}}{\partial y}\bigg|_0 = \frac{\sqrt{j\mu}}{\lambda}(G - H) \quad [24]$$

At the chromate layer/electrolyte interface ($\chi = 1$)

$$\tilde{C}_\lambda = (G\exp\sqrt{j\mu} + H\exp - \sqrt{j\mu}) \quad [25]$$

thus

$$\frac{d\tilde{C}_{H^+}}{dy}\bigg|_{\lambda^-} = \frac{\sqrt{j\mu}}{\lambda}(G\exp\sqrt{j\mu} - H\exp - \sqrt{j\mu}) \quad [26]$$

Chromate layer/zinc interface.—Due to the electrochemical reactions, the nonsteady kinetic equations are

$$\frac{\tilde{i}}{F} = \left\{ \begin{array}{l} [-2(k_1 + k_2) - 2k_{22}\beta C_0^2 + 3k_3[\mathrm{CrO_4^{2-}}]C_0^5 + 2k_4\beta]\tilde{\theta} + \frac{1}{R_t F}\tilde{E} + \\ +[-4k_{22}\beta\theta C_0 - 15k_3(1-\theta)[\mathrm{CrO_4^{2-}}]C_0^4]\tilde{C}_0 \end{array} \right\} \quad [27]$$

where

$$R_t = (F\{2b_1k_1(1-\theta) + 2b_2k_2(1-\theta) + 2b_{22}k_{22}\beta\theta C_0^2 + 3b_3k_3(1-\theta)[\mathrm{CrO_4^{2-}}]C_0^5 + 2b_4k_4\beta\theta\})^{-1} \quad [28]$$

is the charge-transfer resistance. From Eq. 2

$$j\omega\beta\tilde{\theta} = [b_2k_2(1-\theta) + b_{22}k_{22}\beta\theta C_0^2]\tilde{E} - (k_2 + k_{22}\beta C_0^2)\tilde{\theta} - (2k_{22}\beta\theta C_0)\tilde{C}_0 \quad [29]$$

or

$$\tilde{\theta} = A\tilde{E} + B\tilde{C}_0 \quad [30]$$

where

$$A = \frac{b_2k_2(1-\theta) + b_{22}k_{22}\beta\theta C_0^2}{j\omega\beta + k_2 + k_{22}\beta C_0^2}$$

and

$$B = \frac{-2k_{22}\beta\theta C_0}{j\omega\beta + k_2 + k_{22}\beta C_0^2}$$

$$D_f\left.\frac{d\tilde{C}_{H^+}}{dy}\right|_0 = \left\{ \begin{array}{l} [-5b_3k_3(1-\theta)[\mathrm{CrO_4^{2-}}]C_0^5 - 2b_2k_2(1-\theta) + 2b_{22}k_{22}\beta\theta C_0^2]\tilde{E} + \\ +[-5k_3[\mathrm{CrO_4^{2-}}]C_0^5 - 2k_2 + 2k_{22}\beta C_0^2]\tilde{\theta} + \\ +[25k_3(1-\theta)[\mathrm{CrO_4^{2-}}]C_0^4 + 4k_{22}\beta\theta C_0]\tilde{C}_0 \end{array} \right\} = D_f\frac{\sqrt{j\mu}}{\lambda}(G - H) \quad [31]$$

Eq. 17, 18, 23, 25-27, 30, and 31 provide a set of eight equations with eight unknowns (i, θ, C_0, C_λ, $d\tilde{C}_{H^+}/dy|_{\lambda^-}$, $d\tilde{C}_{H^+}/dy|_{\lambda^+}$, G, and H), which can be solved.

The set of eight equations can be simplified through the following steps. Introduction of Eq. 30 into Eq. 31 yields

$$M\tilde{E} + N\tilde{C}_0 = D_f\frac{\sqrt{j\mu}}{\lambda}(G - H) \quad [32]$$

where

$$M = [-5b_3k_3(1-\theta)[\mathrm{CrO_4^{2-}}]C_0^5 - 2b_2k_2(1-\theta) + 2b_{22}k_{22}\beta\theta C_0^2] + A[-5k_3[\mathrm{CrO_4^{2-}}]C_0^5 - 2k_2 + 2k_{22}\beta C_0^2] \quad [33]$$

and

$$N = [25k_3(1-\theta)[\mathrm{CrO_4^{2-}}]C_0^4 + 4k_{22}\beta\theta C_0] + B[-5k_3[\mathrm{CrO_4^{2-}}]C_0^5 - 2k_2 + 2k_{22}\beta C_0^2] \quad [34]$$

Incorporation of Eq. 23 into Eq. 32 yields

$$G = \left(\frac{\lambda M}{2D_f\sqrt{j\mu}}\right)\tilde{E} + \left(\frac{\lambda N}{2D_f\sqrt{j\mu}} + \frac{1}{2}\right)\tilde{C}_0 \quad [35]$$

and

$$H = \left(\frac{-\lambda M}{2D_f\sqrt{j\mu}}\right)\tilde{E} - \left(\frac{\lambda N}{2D_f\sqrt{j\mu}} - \frac{1}{2}\right)\tilde{C}_0 \quad [36]$$

Upon including Eq. 25, 26, 35, and 36 in Eq. 19

$$D_s\left.\frac{d\tilde{C}_{H^+}}{dy}\right|_{\lambda^+} = (M\cosh\sqrt{j\mu})\tilde{E} + \left(N\cosh\sqrt{j\mu} + \frac{D_f\sqrt{j\mu}}{\lambda}\sinh\sqrt{j\mu}\right)\tilde{C}_0 \quad [37]$$

Upon introducing the term $d\tilde{C}_{H^+}/dy|_{\lambda^+}$ (Eq. 17) in Eq. 37

$$(M\cosh\sqrt{j\mu})\tilde{E} + \left(N\cosh\sqrt{j\mu} + \frac{D_f\sqrt{j\mu}}{\lambda}\sinh\sqrt{j\mu}\right)\tilde{C}_0 = \frac{1}{D_s}\left[\frac{\tilde{C}_\lambda\theta'(0)}{\delta} + \frac{\tilde{\Omega}}{\bar{\Omega}}\left.\frac{d\bar{C}_{H^+}}{dy}\right|_{\lambda^+}W_H\right] \quad [38]$$

Finally, introduction of the term $\tilde{C}_\lambda$ of Eq. 25 into Eq. 38 yields

$$\tilde{C}_0 = \frac{\frac{1}{\cosh\sqrt{j\mu}}\frac{\tilde{\Omega}}{\bar{\Omega}}\left.\frac{d\bar{C}_{H^+}}{dy}\right|_{\lambda^+}W_H\frac{1}{D_s} - M\left\{1 + \frac{\lambda}{D_f}\frac{\tanh\sqrt{j\mu}}{\sqrt{j\mu}}\left[\frac{-\theta'(0)}{\delta}\frac{1}{D_s}\right]\right\}\tilde{E}}{N + \frac{Df\sqrt{j\mu}}{\lambda}\tanh\sqrt{j\mu} + \left(\frac{\lambda N}{D_f}\frac{\tanh\sqrt{j\mu}}{\sqrt{j\mu}} + 1\right)\left[\frac{-\theta'(0)}{\delta}\frac{1}{D_s}\right]} \quad [39]$$

AC impedance model.—To obtain an expression for electrochemical impedance, Eq. 30 is incorporated into Eq. 27 to provide

$$\frac{\tilde{i}}{F} = [-2(k_1 + k_2) - 2k_{22}\beta C_0^2 + 3k_3[\mathrm{CrO_4^{2-}}]C_0^5 + 2k_4\beta] \times(A\tilde{E} + B\tilde{C}_0) + \frac{1}{R_tF}\tilde{E} + [-4k_{22}\beta\theta C_0 - 15k_3(1-\theta) \times[\mathrm{CrO_4^{2-}}]C_0^4]\tilde{C}_0 \quad [40]$$

and the faradaic impedance ($1/Z_F = \tilde{i}/\tilde{E}$) becomes

$$\frac{\tilde{i}}{\tilde{E}} = F\left\{ \begin{array}{l} [-2(k_1 + k_2) - 2k_{22}\beta C_0^2 + 3k_3[\mathrm{CrO_4^{2-}}]C_0^5 + 2k_4\beta] \\ \quad \times\left(A + B\frac{\tilde{C}_0}{\tilde{E}}\right) + \frac{1}{R_tF} + \\ +[-4k_{22}\beta\theta C_0 - 15k_3(1-\theta)[\mathrm{CrO_4^{2-}}]C_0^4]\frac{\tilde{C}_0}{\tilde{E}} \end{array} \right\} \quad [41]$$

For the electrochemical impedance the rotation speed modulation is zero ($\tilde{\Omega} = 0$), thus Eq. 39 becomes

$$\frac{\tilde{C}_0}{\tilde{E}} = \frac{-M\left\{1 + \frac{\lambda}{D_f}\frac{\tanh\sqrt{j\mu}}{\sqrt{j\mu}}\left[\frac{-\theta'(0)}{\delta}\frac{1}{D_s}\right]\right\}}{N + \frac{D_f\sqrt{j\mu}}{\lambda}\tanh\sqrt{j\mu} + \left(\frac{\lambda N}{D_f}\frac{\tanh\sqrt{j\mu}}{\sqrt{j\mu}} + 1\right)\left[\frac{-\theta'(0)}{\delta}\frac{1}{D_s}\right]} \quad [42]$$

The total impedance (Z_T) expression of the system is

$$Z_T = \frac{1}{\frac{1}{Z_F} + j\omega C_d} \quad [43]$$

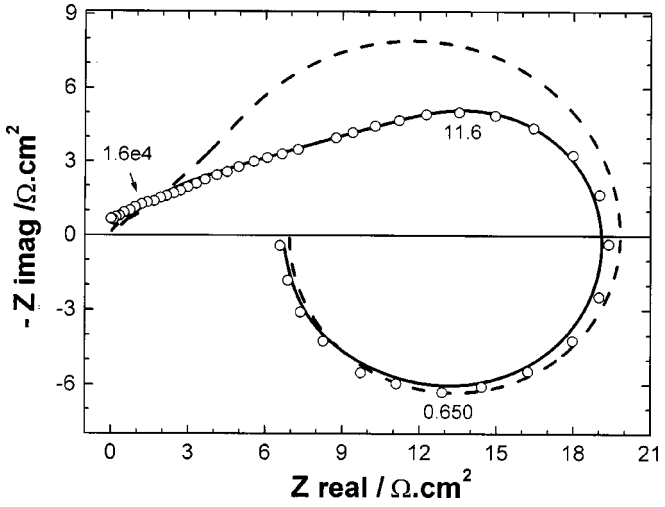

Figure 6. Comparison between simulated electrochemical impedance diagrams obtained with (——) Z_{deLevie}, (— — —) without Z_{delevie}, and (○) experimental impedance obtained after 15 min immersion in the solution at 47°C at 1000 rpm (frequencies in hertz).

where C_d is the dl capacitance.

In the experimental impedance diagrams, the high frequency part of the second capacitive loop, which has the appearance of a diffusion impedance, does not exhibit an angle of 45° with respect to real-axis but, rather, an angle close to 22.5°. To provide a better match between simulations and experiments, it was necessary to take into account this behavior which may be linked to the 3-D geometry of a zinc electrode (roughness or porosity). For the porous model of de Levie,[25] when the pore is considered as semi-infinite the overall impedance varies as $Z^{1/2}$ where Z is the corresponding impedance on a plane electrode. It was shown that this behavior is the same for all pore geometry.[26] In a potential and/or concentration distribution along the pore the model is much more complex, Los and Hitz *et al.* proposed the use of two constant phase elements (CPEs) to take this distribution into account.[27,28] In the present case, to limit the number of unknown parameters we prefer to consider that the overall impedance is proportional to the square root of the total impedance given by expression 43

$$Z_{ac} = KZ_T^{1/2} \qquad [44]$$

where K is a constant. The dissolution of zinc does not occur on plan-to-plan but on the walls of a semi-infinite porous medium,[29,30] and in the present case clearly the diffusive impedance responses do not have an angle of 45° with respect to real axis as is shown in Fig. 6. It can be seen that it is necessary to consider $Z_T^{1/2}$ to simulate the capacitive diffusion loops detected in the experimental results.

EHD impedance model.—The simulation of electrohydrodynamical impedance takes into account simultaneously, but separately, the anodic and cathodic reactions in the process of formation of the film. So it is necessary to separate the anodic and cathodic influence from the total steady-state faradaic current. The anodic steady-state faradaic current is

$$\frac{i_a}{F} = 2k_1(1-\theta) + 2k_2(1-\theta) + 2k_4\beta\theta \qquad [45]$$

and the cathodic is

$$\frac{i_c}{F} = -2k_{22}\beta\theta C_0^2 - 3k_3(1-\theta)[CrO_4^{2-}]C_0^5 \qquad [46]$$

The nonsteady kinetic equations under potentiostatic control ($\tilde{E} = 0$) is, for the anodic part

$$\frac{\tilde{i}_a}{F} = [-2(k_1 + k_2) + 2k_5\beta]\tilde{\theta} \qquad [47]$$

and, for the cathodic part

$$\frac{\tilde{i}_c}{F} = [-2k_{22}\beta C_0^2 + 3k_3[CrO_4^{2-}]C_0^5]\tilde{\theta} + [-4k_{22}\beta\theta C_0 - 15k_3(1-\theta)[CrO_4^{2-}]C_0^4]\tilde{C}_0 \qquad [48]$$

Eq. 30 for $\tilde{E} = 0$ becomes

$$\tilde{\theta} = B\tilde{C}_0 \qquad [49]$$

where

$$= \frac{-2k_{22}\beta\theta C_0}{j\omega\beta + k_2 + k_{22}\beta C_0^2} \qquad [50]$$

and Eq. 39 becomes

$$\tilde{C}_0 = \frac{\dfrac{1}{\cosh\sqrt{j\mu}}\dfrac{\tilde{\Omega}}{\bar{\Omega}}\left.\dfrac{d\bar{C}_{H^+}}{dy}\right|_{\lambda^+} W_H\dfrac{1}{D_s}}{N + \dfrac{Df\sqrt{j\mu}}{\lambda}\tanh\sqrt{j\mu} + \left(\dfrac{\lambda N}{D_f}\dfrac{\tanh\sqrt{j\mu}}{\sqrt{j\mu}} + 1\right)\left(\dfrac{-\theta'(0)}{\delta}\dfrac{1}{D_s}\right)} \qquad [51]$$

$$\text{where } N = [25k_3(1-\theta)[CrO_4^{2-}]C_0^4 + 4k_{22}\beta\theta C_0] + B[-5k_3[CrO_4^{2-}]C_0^5 - 2k_2 + 2k_{22}\beta C_0^2] \qquad [52]$$

Including the term $\tilde{\theta}$ (Eq. 51) in Eq. 47 and 48, expressions are obtained for the anodic EHD influence

$$Z_{EHD_a} = \frac{\tilde{i}_a}{\tilde{\Omega}} = F\left\{[-2(k_1 + k_2) + 2k_4\beta]B\frac{\tilde{C}_0}{\tilde{\Omega}}\right\} \qquad [53]$$

and the cathodic influence

$$Z_{EHD_c} = \frac{\tilde{i}_c}{\tilde{\Omega}} = F\left\{([-2k_{22}\beta C_0^2 + 3k_3[CrO_4^{2-}]C_0^5]B + [-4k_{22}\beta\theta C_0 - 15k_3(1-\theta)[CrO_4^{2-}]C_0^4])\frac{\tilde{C}_0}{\tilde{\Omega}}\right\} \qquad [54]$$

The total EHD (Z_{EHD_T}) is obtained by the sum of anodic and cathodic EHD impedances divided by the same impedance in the low dimensionless frequency limit.

$$\frac{Z_{EHD_T}(p)}{Z_{EHD_T}(0)} = \frac{\left(\dfrac{\tilde{i}_a}{\tilde{\Omega}}(p) + \dfrac{\tilde{i}_c}{\tilde{\Omega}}(p)\right)}{\left(\dfrac{\tilde{i}_a}{\tilde{\Omega}}(0) + \dfrac{\tilde{i}_c}{\tilde{\Omega}}(0)\right)} \qquad [55]$$

The simulations of Z_{ac} obtained for the set of parameters show in Tables I-IV are given in Fig. 7. The parameters k_{30} and C_0 were

calculated by Eq. 8 and 11, respectively. The parameter k_3 varies between 2.5×10^{15} and 5.0×10^{15}, and C_0 varies between 4.8×10^{-5} and 6.38×10^{-5} M. These variations depend on the potential and the rotation speed of the electrode. The values of C_0 yield a variation of pH between 4.32 and 4.20, which are consistent with the experimental results obtained by local pH measurements (Fig. 4) that represent the pH measured at the chromate layer/electrolyte interface. The convective diffusion coefficient D_s is 10^{-4} cm^2 s^{-1}. The chromate layer diffusion coefficient that corresponds to the experimental conditions at 25°C is 3.3×10^{-8} cm^2 s^{-1}, at 47°C the diffusion coefficient is assumed to be 6.1×10^{-8} cm^2 s^{-1}, considering that increases of temperature increase the diffusion in a gel-like film.

It is shown in Fig. 7a and b that the impedance increases for the same rotation speed with the increase of chromate layer thickness, and it is directly proportional to immersion time in the chromate bath as shown in experimental results (Fig. 2a and b). The Z_{ac} simulation in Fig. 7c and d, analogous to the experimental results with rotation speed variation for the same immersion time (Fig. 2c and d), were obtained by the variation of chromate and convective electrolyte layer thickness. The decrease of chromate layer thickness with increase of rotation rate was assumed because the layer is presumed to be a gel-like film, and the convective electrolyte layer thickness calculated by Eq. 14 is inversely proportional to rotation speed.

The simulations of Z_{EHD} were obtained with the same set of parameters used for the Z_{ac} simulations, but in this case the anodic and cathodic effects were analyzed independently. The cathodic and anodic currents in function of electrode rotation rates calculated by

Table I. Reaction rates parameters k_{io} (mol cm^{-2} s^{-1}) used for ac and EHD impedance simulations. k_{30} is claculated by Eq. 4.

k_{10}	k_{20}	k_{220}	k_{40}
8.0×10^{-1}	2.6×10^{10}	2.1×10^{-16}	1.4×10^{11}

Table II. Kinetic parameters b_i used for ac and EHD impedance simulations in function of solution temperatures from experimental results.

Temperature (°C)	b_1 (V^{-1})	b_2 (V^{-1})	b_{22} (V^{-1})	b_3 (V^{-1})	b_4 (V^{-1})
25	18.0	37.8	40.0	3.0	30.0
47	16.8	35.3	37.3	2.8	28.0

Table III. Chromate layer thickness and parameters used for the simulations of experimental impedances at 1000 rpm in function of immersion times, solution temperatures, and electrode potentials.

Temperature (°C)	Immersion time (min)	E (V)	λ (cm)
25	2	−1.309	2.0×10^{-5}
	15	−1.317	5.0×10^{-5}
	30	−1.319	7.0×10^{-5}
47	2	−1.320	2.2×10^{-5}
	15	−1.322	5.7×10^{-5}
	30	−1.324	7.8×10^{-5}

Table IV. Chromate layer thickness and parameters used for the simulations of experimental impedances at 30 min in function of rotation speed, solution temperatures, and electrode potentials.

Temperature (°C)	Rotation speed (rpm)	E (V)	λ (cm)
25	250	−1.325	9.4×10^{-5}
	500	−1.322	8.7×10^{-5}
	1000	−1.319	7.0×10^{-5}
47	250	−1.325	10.5×10^{-5}
	500	−1.324	8.2×10^{-5}
	1000	−1.324	7.8×10^{-5}

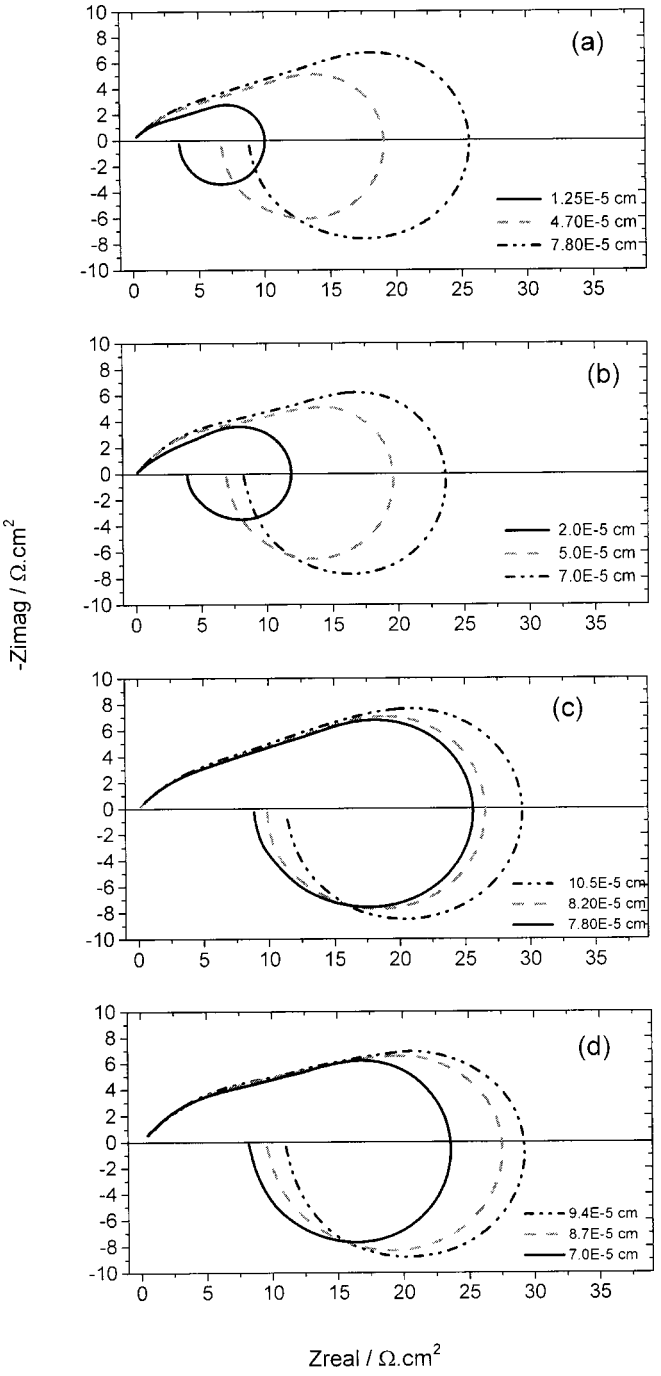

Figure 7. Simulated electrochemical impedance diagrams at 1000 rpm for different chromate layers thickness (legends) corresponding to the experimental temperature condition of (a) 47°C and (b) 25°C and simulated diagrams obtained for different chromate layers thickness (legends) at 250 rpm (— — —), at (gray dashes) 500 rpm, and (——) 1000 rpm corresponding to experimental temperature condition of (c) 47°C and (d) 25°C after 30 min (frequencies in hertz).

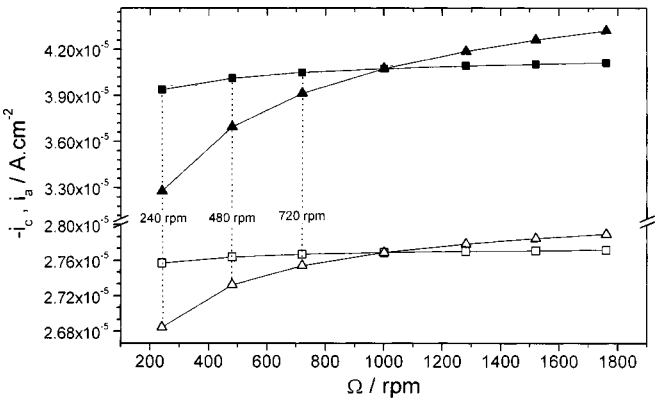

Figure 8. (square symbols) Anodic and (triangle symbols) cathodic currents in function of rotation speed simulated for temperatures conditions of (open symbols) 25 and (solid symbols) 47°C.

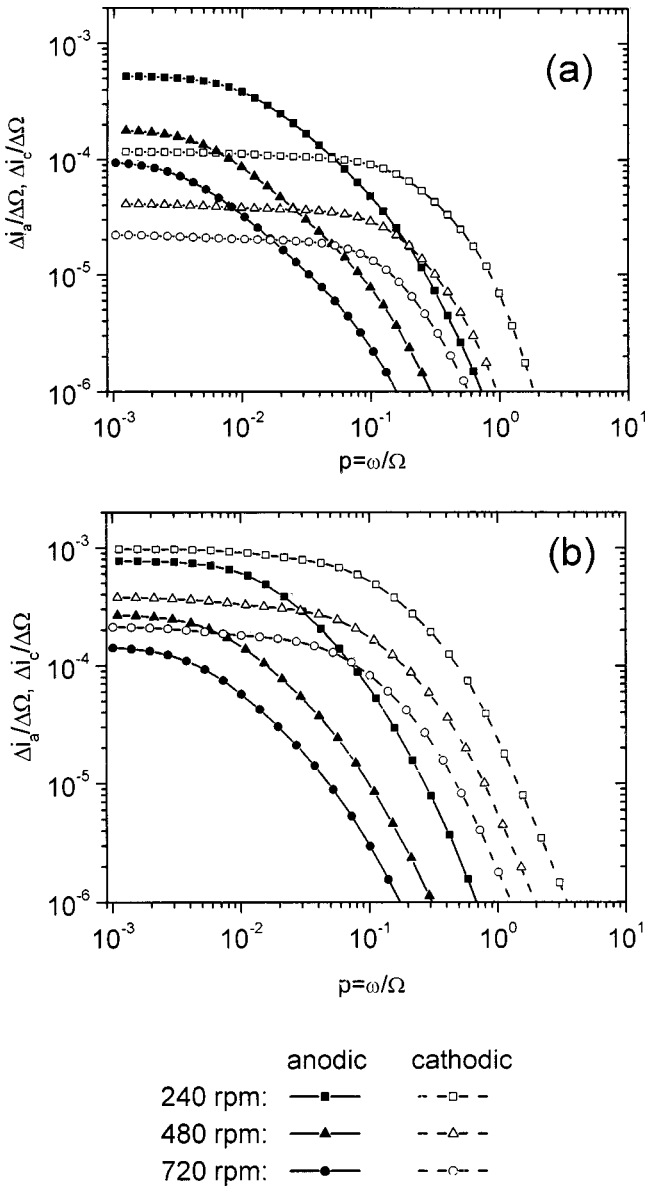

Figure 9. Anodic and cathodic EHD in function of rotation speed simulated corresponding to the experimental temperature conditions of (a) 25 and (b) 47°C.

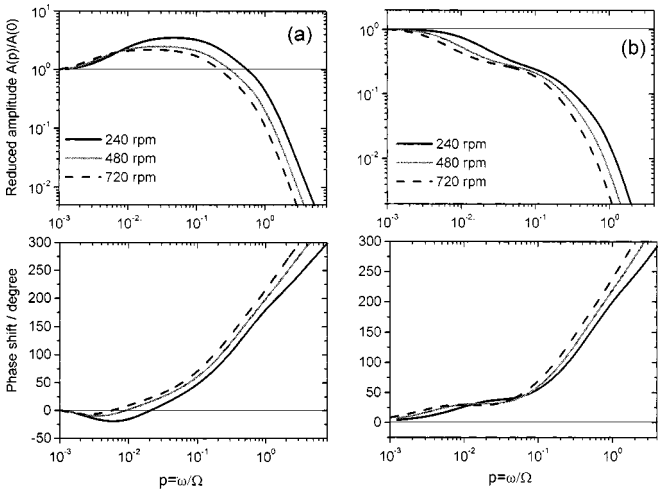

Figure 10. Simulated total EHD diagrams corresponding to the experimental conditions of (a) 47 and (b) 25°C.

Eq. 45 and 46 are presented in Fig. 8. These simulations were obtained by the variation of rotation rates with fixed potentials correspondent to a rotation rate of 1000 rpm at 25 and 47°C. The current shifts are larger when rotation speeds decrease and for the conditions of 47°C are greater than 25°C. The nonnormalized modulus of EHD of cathodic and anodic parts calculated by Eq. 53 and 54 are presented in Fig. 9, the Schmidt number corresponding to H^+ diffusion used to simulate the experimental conditions was 100 at 25°C and 50 at 47°C. The calculations allow identification of the different effects of cathodic and anodic reactions in the electrohydrodynamical behavior in the zinc interface with a chromate film formed in a way that cannot be observed by experimental results. The behavior of the cathodic curves in terms of modulus values is completely different between the temperature conditions simulated. The changes are due to the temperature dependence of H^+ diffusion coefficient and to the current shifts show in Fig. 8. When the cathodic and anodic electrohydrodynamical effects are combined into the total EHD of the system (Eq. 55), the responses are obtained (Fig. 10) that are equivalent to experimental results (Fig. 3). The diagrams shown in Fig. 10b are analogous to those obtained in experimental conditions at 25°C, showing the same two constant times, the diagrams being shifted toward lower values as rotation rate is increased, and phase curves that increase continuously. The simulated diagrams of Fig. 10a are in good agreement with their analogous experimental diagrams at 47°C. They present the same ''hump'' in intermediary frequencies that is the beginning of the total response of the oxidization of zinc and the reduction of Cr^{6+} on the surface of zinc.

Conclusions

Based on the above results and discussion, the following points can be outlined: (*i*) the Z_{ac} simulation based with only four reactions and the mass-transport model proposed for the chromatation reactions on zinc are in good agreement with the different experimental results; (*ii*) the Z_{EHD} simulation of the separation of anodic and cathodic reactions effects was favorable for explain the electrohydrodynamical behavior for different conditions of chromate formation. This aspect seems to have fundamental importance in the kinetic role of the chromatation process and could be key as a future candidate of nontoxic conversion baths.

Acknowledgments

The Brazilian authors thank CNPq, FAPERJ, CAPES, and FUJB. The authors express their thanks to Mark Orazem for his critical reading of the manuscript.

The Federal University of Rio de Janiero assisted in meeting the publication costs of this article.

List of Symbols

a	constant (0.51023)
b_i	kinetic parameter of reaction i, V^{-1}
C	concentration of H^+, mol cm^{-3}
C_d	double layer capacitance, F cm^{-2}
D	diffusion coefficient, cm^2 s^{-1}
E	overall potential, V
F	Faraday number (96,487 C/equiv)
f'	nonsteady dimensionless function corresponding to the radial velocity gradient
G	integration constant (Eq. 22)
H	integration constant (Eq. 22)
i	current density, A/cm^2
j	$(-1)^{1/2}$
K	$Z_{\text{de Levie}}$ constant
k_{i0}	reaction rates of reaction i, mol cm^{-2} s^{-1}
p	dimensionless frequency (ω/Ω)
R	universal gas constant (8.3143 J/mol K)
Re	Reynolds number
R_t	charge-transfer resistance, Ω
Sc	Schmidt number
t	time, s
V_y	normal velocity, cm/s
W_H	transfer function tabulated in Ref. 23, 24 as $W_0(\xi)$
y	normal coordinate, cm
Z_{ac}	ac impedance
$Z_{\text{de Levie}}$	de Levie impedance (Eq. 44)
Z_{EHD}	electrohydrodynamic impedance, C

Greek

β	total number of sites available for adsorption
Γ	gamma function
δ	convective diffusion layer thickness, cm
η	axial dimensionless distance (y/δ)
θ	coverage fraction
$-1/\theta'(0)$	dimensionless convective diffusion impedance
λ	chromate layer thickness, cm
μ	dimensionless frequency ($\omega\lambda^2/D_f$)
ξ	dimensionless frequency ($3.57\ pSc^{1/3}$)
ρ	electrolyte resistivity, Ω cm
υ	kinematic viscosity, cm^2 s^{-1}
χ	axial dimensionless distance (y/λ)
ω	pulsation, s^{-1}
Ω	angular velocity, rd s^{-1}

Subscripts

f	relative to chromate layer
H^+	relative to H^+ species
o	at the electrode surface
s	relative to convective diffusion layer
λ	at the interface chromate layer/electrolyte
∞	in the bulk solution

Superscripts

$-$	mean value
$\sim$	complex quantity of small amplitude

References

1. A. A. O. Magalhães, I. C. P. Margarit, and O. R. Mattos, *Electrochim. Acta*, **44**, 4281 (1999).
2. A. Pirnát, L. Mészáros, G. Mészáros, and B. Lengyel, *Corros. Sci.*, **34**, 1147 (1993).
3. C. Marikkannu, V. Sudaram, and B. Venkataraman, in *Proceedings of the 10th International Corrosion Congress*, Vol. 1, p. 1333 (Nov 1987) (Oxford & IBH, New Delhi.
4. R. L. Zeller III and R. F. Savinell, *Corros. Sci.*, **26**, 389 (1986).
5. L. Fedrizzi and F. Marchetti, *J. Mater. Sci.*, **26**, 1931 (1991).
6. M. El-Sharif, Y. Su, C. Chisholm, and A. Watson, *Corros. Sci.*, **35**, 1259 (1993).
7. J. Hazan, C. Coddet, and M. Keddam, *Corros. Sci.*, **31**, 313 (1990).
8. L. Fedrizzi, L. Ciaghi, L. Bonora, R. Fratesi, and G. Roventi, *J. Appl. Electrochem.*, **22**, 247 (1992).
9. K. G. MacLaren, J. H. Green, and A. H. Kingsbury, *Corros. Sci.*, **1**, 161 (1961).
10. J. P. G. Farr and S. V. Kulkarni, *Trans. Inst. Met. Finish.*, **44**, 21 (1966).
11. L. F. G. Willians, *Surf. Technol.*, **4**, 355 (1976).
12. J. R. Ducan, *Surf. Technol.*, **16**, 163 (1982).
13. L. F. G. Willians, *Surf. Technol.*, **5**, 355 (1977).
14. H. E. Biber, *Metall. Trans. A*, **19**, 1609 (1988).
15. C. V. Bishop, D. M. Burdt, and K. R. Romer, *Galvanotechnik*, **71**, 1199 (1980).
16. M. P. Gigandet, J. Faucheu, and M. Tachez, *Surf. Coat. Technol.*, **89**, 285 (1997).
17. C. Deslouis, I. Frateur, G. Maurin, and B. Tribollet, *J. Appl. Electrochem.*, **27**, 482 (1997).
18. E. L'Hostis, C. Deslouis, B. Tribollet, and D. Festy, *Electrochim. Acta*, **41**, 1393 (1996).
19. F. X. Perrin, M. P. Gigandet, M. Wery, and J. Pagetti, *Surf. Coat. Technol.*, **105**, 135 (1998).
20. J. D. Ramsey, L. Xia, M. W. Kending, and R. L. McCreery, *Corros. Sci.*, **43**, 1557 (2001).
21. L. Xia and R. L. McCreery, *J. Electrochem. Soc.*, **145**, 3083 (1998).
22. S. L. Díaz, O. R. Mattos, O. E. Barcia, and F. J. F. Miranda, *Electrochim. Acta*, **47**, 4091 (2002).
23. B. Tribollet and J. Newman, *J. Electrochem. Soc.*, **130**, 2016 (1983).
24. C. Deslouis and B. Tribollet, in *Advances in Electrochemical Science and Engineering*, C. W. Tobias and H. Gerischer, Editors, Vol. 2, p. 205, VCH Weinhein, New York (1991).
25. R. de Levie, *Adv. Electrochem. Electrochem. Eng.*, **6**, 329 (1967).
26. J. P. Pierre, P. Fouilloux, M. Keddam, and H. Takenouti, *Electrochim. Acta*, **26**, 1029 (1981).
27. P. Los, A. Lasia, L. Brossard, and H. Ménard, *J. Electroanal. Chem.*, **360**, 101 (1993).
28. C. Hitz and A. Lasia, *J. Electroanal. Chem.*, **500**, 213 (2001).
29. C. Cachet, B. Saidani, and R. Wiart, *J. Electrochem. Soc.*, **139**, 644 (1992).
30. L. Sziraki, E. Szoocs, Zs. Pilbath, K. Papp, and E. Kalman, *Electrochim. Acta*, **46**, 3743 (2001).